The Fractal Geometry of Patterned Structures in Numerical Models of Rock Deformation

Alison Ord
CSIRO Division of Exploration and Mining,
Private Bag, PO Wembley, WA 6014, Australia

'... and I doubt that we are founding a new science, but at least we are having fun.'
Nonlinear dynamics, chaos and mechanics. P. Holmes, 1990

Abstract. Geologic structures are repetitive in a quasi-periodic or erratic manner. The geometries of these structures are also manifestations of the mechanical behaviour of a deforming rock mass. Can we therefore obtain information on the *dynamics* of a complex geologic system from an examination of the *geometry* of geologic structures? We examine this question from the point of view of non-linear dynamics.

We investigate the variability in space of the velocity of growth of crenulations in a model rock mass which is undergoing a (numerical) simple shearing deformation. That is, we follow the distribution and evolution of the velocity in space, rather than in time. We investigate the thesis that the behaviour of this one variable reflects the presence of all other variables participating in the dynamics and, by use of increasing multiples of a fixed space lag, discretize the system, and unfold the system's dynamics into a multidimensional phase space. The trajectories within this phase space of the system converge to a subspace which is the geometrical attractor for the system. We infer from this that our deforming model rock can be described by a set of deterministic laws. The dimension of this attractor is about 2.5; that is, the system may be completely represented by a fractal attractor. Further, this fractal attractor embeds in a phase space of three so that at least three variables must be considered in the description of the underlying dynamics. These are the variables involved in the three independent differential equations of the numerical model: the stress equations of motion, the yield criterion and the flow rule. We conclude that geological systems may be successfully modelled on the basis of such a system of equations, and analysed using the concepts of fractal geometry.

This new application of nonlinear dynamics to the spatially erratic structures of deformed rocks results in an improved understanding of rock deformation behaviour and in an improved prediction of the distributions of structurally-controlled phenomena.

Introduction

The patterns observed in geological structures such as crenulations, crenulation cleavages, and shear zones are typically arranged in ways which are close to, but not strictly, periodic. In this chapter, we shall refer to these patterns as quasi-periodic. Chaos is an attribute of any system which is extremely sensitive to

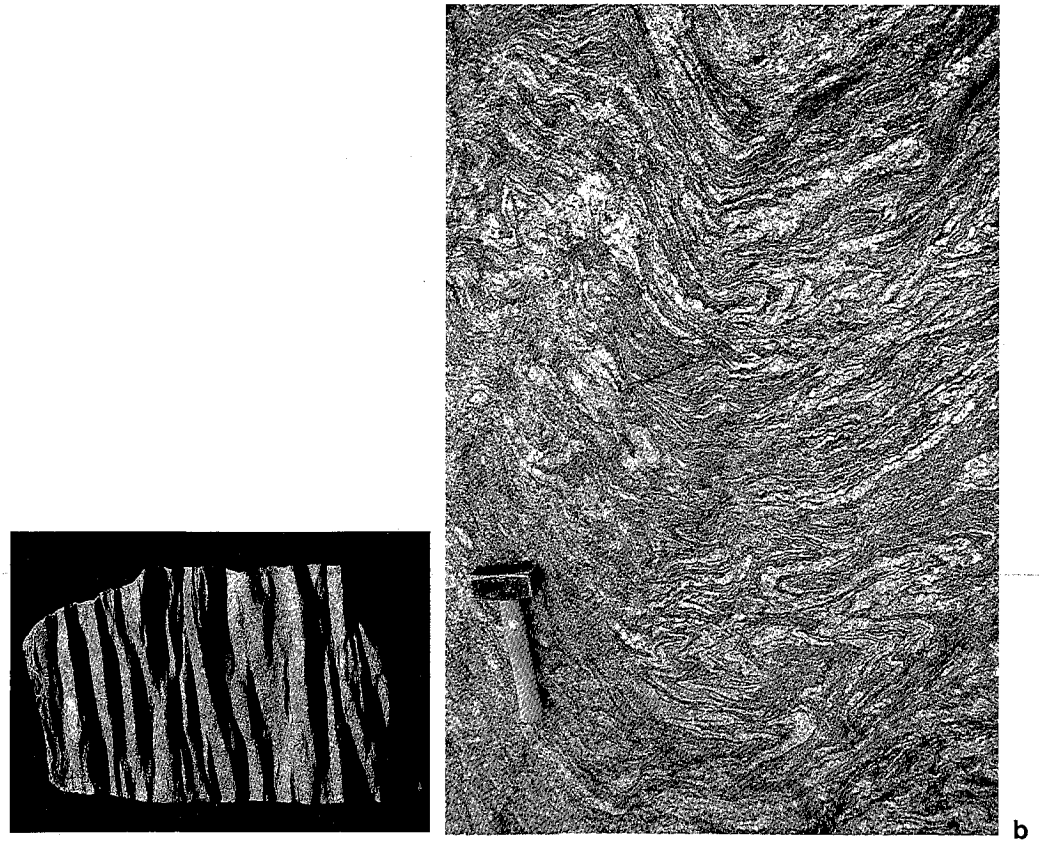

Fig. 1. a. Deformed, crenulated rock with quasi-periodic spatial distribution of fold axes. Maximum dimensions are 13 x 8 cm. **b.** Multiple pegmatite intrusion and folding during progressive deformation. Albany Mobile Belt, Southern Domain migmatitic gneiss, Western Australia. Hammer length is 30 cm. Photograph by Lyal Harris.

initial conditions. In general, this means that adjacent points behave quite differently in time and space. In the quasi-periodic structures characteristic of most deformed rocks, strict chaos, in either time or space, is unlikely because adjacent points in the deforming body commonly follow closely-related paths in time and space throughout their history in order to preserve the continuity of the deforming rock mass. Although rock masses such as that shown in Fig. 1a are irregular, they are not chaotic because adjacent points have followed closely-related deformation paths. However, the geometric structures observed in multiply-deformed terrains associated with migmatites (Fig. 1b) are of the highly

irregular and multiply-stretched and folded nature of chaotic systems. The patterning of these quasi-periodic structures in space is analogous to the patterning in time of, for example, electroencephalograms (Albano et al. 1986) and the responses in some electrical systems (Van der Pol 1927). More erratic or chaotic phenomena include the weather (Lorenz 1963, 1979) and Couette flow (Gollub & Swinney 1975). Geological phenomena which have been observed and analysed to be patterned in time include earthquakes (Hobbs 1990), volcanic tremor and gas piston events (Chouet & Shaw 1991) and volcanic eruptions (Sornette et al. 1991).

Quasi-periodicity and chaos may be described as natural phenomena associated with the behaviour of a dynamic, self-organising system. The thesis here is that a deforming rock is as much such a dynamic, self-organising system as is the weather or the more controlled example of Couette flow and is therefore amenable to the same analytic techniques. However, in geology as in all other disciplines, sets of linear differential equations are simpler to solve than sets of non-linear differential equations, so that until now, geological structures have been analysed in terms of strictly periodic or regular patterns (e.g. Biot 1961, Ramberg 1964).

It is therefore considered feasible to analyse geological structures using the mathematical techniques developed in discussions of theories describing temporally patterned phenomena, and in the practical analysis of the resultant data. We describe here the data resulting from a simple numerical model for a deforming rock mass, and construct a spatial attractor for the spatially-disposed pattern in a manner analogous to that in which Packard et al. (1980, see also Takens 1981, Crutchfield et al. 1986) obtained the attractor for a temporally-disposed system.

We need to quantify the information contained in the attractor. Here, we do this by determining the dimension of the spatial attractor for the system through description of the attractor in different embedding dimensions. A collection of points produced by a random process will always tend to fill space so that, for n-dimensional space, the dimension of this collection of points will be close to n. However, for a structured system, as n increases, the attractor of the system will not increasingly fill space, and its dimension will become independent of n. This saturated dimension is then the dimension of the system. If this dimension is fractal (Mandelbrot 1977), then, by comparison with Lorenz's (1963) discovery of a 'strange attractor', the phenomenon is worth further investigation. Its dimension may then indicate the minimum state space needed to reproduce the attractor, and further investigation of its topological behaviour may lead to significant new theoretical results, as well as applications; for example, prediction of the distributions of vein-hosted ore deposits. In particular, the importance of the true dimension of the attractor is that it reflects the number of degrees of freedom of the system, and this number is indicative of the number of independent first-order, nonlinear, differential equations which govern the system.

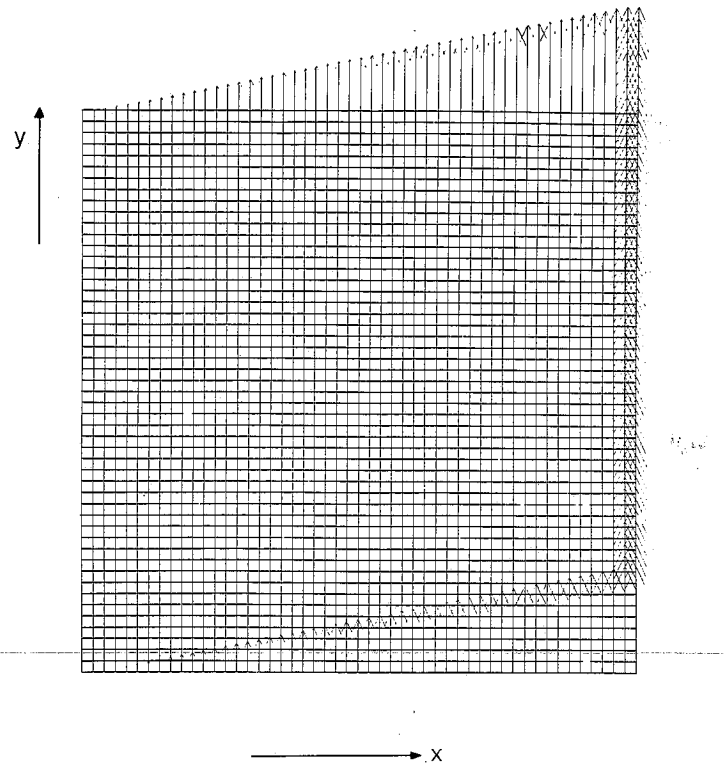

Fig. 2. Finite difference grid of 50 x 50 zones. The arrows represent the direction and relative magnitudes of the velocities applied to the external nodes throughout the deformation.

The aim of this work is therefore to determine and improve information on the constitutive behaviour of rock masses and on the governing equations for rock deformation, from observations of the geometry of geological structures. For example, for description of a simply deforming, non-hardening rock mass, we know that we have interaction between the stress equations of motion, the yield criterion, and the flow rule. Here the dimension of the resulting spatial attractor is expected to be between 1 and 3. Further relationships are required to model more sophisticated behaviour such as strain-hardening or softening, volume change with deformation, coupling of volume change and permeability, fluid flow

coupled with deformation, stress dependence of grain size, and so on. Incorporation of the equations describing these additional phenomena may be required to increase the dimension of the attractor established for the numerical models up to that of the attractor observed for natural systems.

The recognition that the state of such a system may be measured by its fractal dimension provides a new, exciting and rigorous framework within which to improve our understanding of how rock deforms and to understand and to predict the patterning of geological structures.

We first describe the development of a quasi-periodic crenulated structure using a numerical model, and indicate the input and output of this model. Second, we describe how we construct a spatial attractor for the model. A method for calculation of the dimension of the spatial attractor is then summarised. Third, we apply this methodology to analysis of the numerical data, and fourth, we discuss the results in terms of the interaction of the equations describing the numerical model, and consider the application of this method to naturally deformed rocks.

The Model

Numerical modelling of a non-hardening, frictional-dilatant, Mohr-Coulomb material undergoing a simple shearing deformation history results in patterned shear band formation exhibiting both temporally and spatially weakly chaotic or quasi-periodic behaviour (Ord 1990). Similar behaviour is observed also by Cundall (1989, 1991) and by Hobbs & Ord (1989) for constant velocity, plane strain shortening.

The computer code FLAC (Fast Lagrangian Analysis of Continua, Cundall & Board 1988) is used for simulation of rock deformation behaviour. FLAC is a plane-stress or plane-strain explicit finite difference code based upon a Lagrangian calculation scheme suitable for modelling the non-linear behaviour and the large deformation characteristic of geologic structures. It incorporates the basic governing equations for a solid body, that is, the stress equations of motion and the constitutive relations. Further details may be obtained from Board (1989) and FLAC (1991). Physical conditions required for localization in geological materials are discussed and reviewed by Hobbs et al. (1991) who also describe some examples modelled by FLAC.

In FLAC (FLAC 1991) a dynamic relaxation type scheme is employed. In any one time step, new velocities and displacements are derived from stresses and forces through the equations of motion. Strain rates are then derived from the velocities, and new stresses from these strain-rates according to the stress/strain rate relationship (constitutive law) for the deforming material.

The basic equation of motion used is:

$$m\dot{v} = F,$$

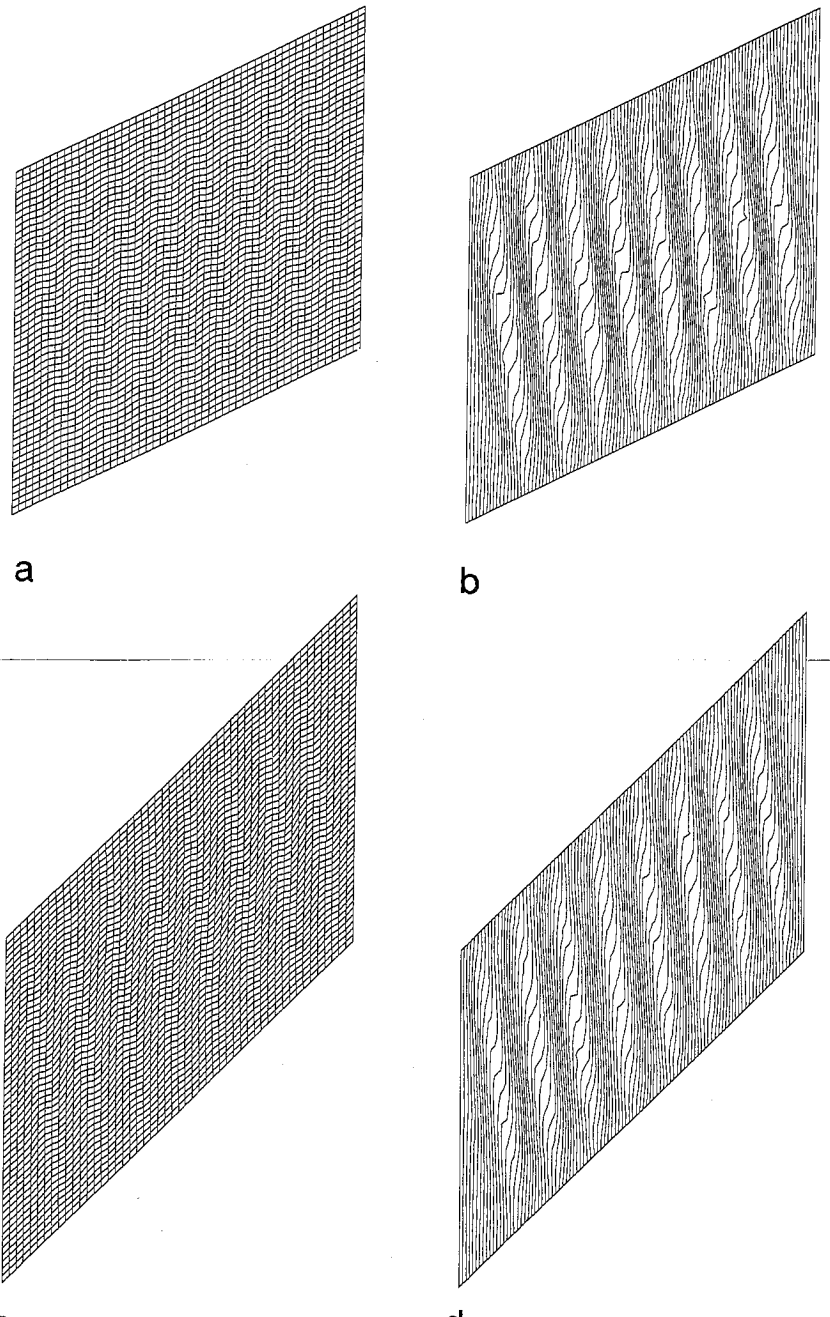

Fig. 3 a-d. 50 x 50 grid (**a**) and (**b**) $\gamma = 0.5$. (**c**) and (**d**) $\gamma = 1.0$. (**a**) and (**c**) Sheared grids. (**b**) and (**d**) Contours of the instantaneous y-velocity. The contour interval is 2.5×10^{-5} units per time step in each case.

which describes a mass, m, which is moved at an acceleration, $\dot{v}$ by a force, F, which may vary with time, t.

The generalised stress equations of motion are:

$$\rho \dot{v}_i = \frac{\partial \sigma_{ij}}{\partial x_j} + \rho g_i$$

for ρ the mass density, x_i the components of the position vector, g_i the components of gravitational acceleration, and σ_{ij} the components of the stress tensor. Indices i,j denote components in a Cartesian coordinate frame, and summation is implied for repeated indices in an expression.

The strain rate is then derived from the velocity gradient according to

$$D_{ij} = \frac{1}{2}\left[\frac{\partial v_i}{\partial x_j} + \frac{\partial v_j}{\partial x_i}\right],$$

for D_{ij} the stretching components and v_i the velocity components.

Finally, the stress is derived from the strain rate according to a constitutive law which is of the form (FLAC, 1991, Eq. 3-4)

$$\sigma_{ij} := M(\sigma_{ij}, D_{ij}, \kappa)$$

where M(...) is the functional form of the constitutive law, κ is an optional history parameter or set of parameters, and : = means 'defined by'.

The external loading is increased sufficiently slowly so that at each time step, the artificial dynamics of the relaxation scheme can be considered as decayed or subsided.

The interest here is the simplicity and known basis of the numerical model in contrast to the complexity and unknown basis of geological structures.

Geometry and Boundary Conditions

The finite difference grid chosen for most of these simple shearing deformation history experiments contains n x n zones. n needs to be large for any analysis of the data to be of use in terms of fractal geometry. In this case, we investigate the effects of having n equal to 50, 100 and 240. In order to bridge the gap with analysis of a time series, we also investigate a grid of 10 000 x 10 zones (n x m). The corners of each zone are defined by nodes. The left hand column of nodes in Fig. 2 was given zero velocity while the most extreme right hand column of nodes was given a velocity of $n \times 10^{-4}$ units per time step, parallel to y, where a unit is the length of an initial element. The rows of external nodes between the outermost columns were given velocities varying from 1 to $(n - 1) \times 10^{-4}$ units per time step so that, together with the condition of plane strain, the bulk deformation was constrained to be isochoric (constant volume). The remaining

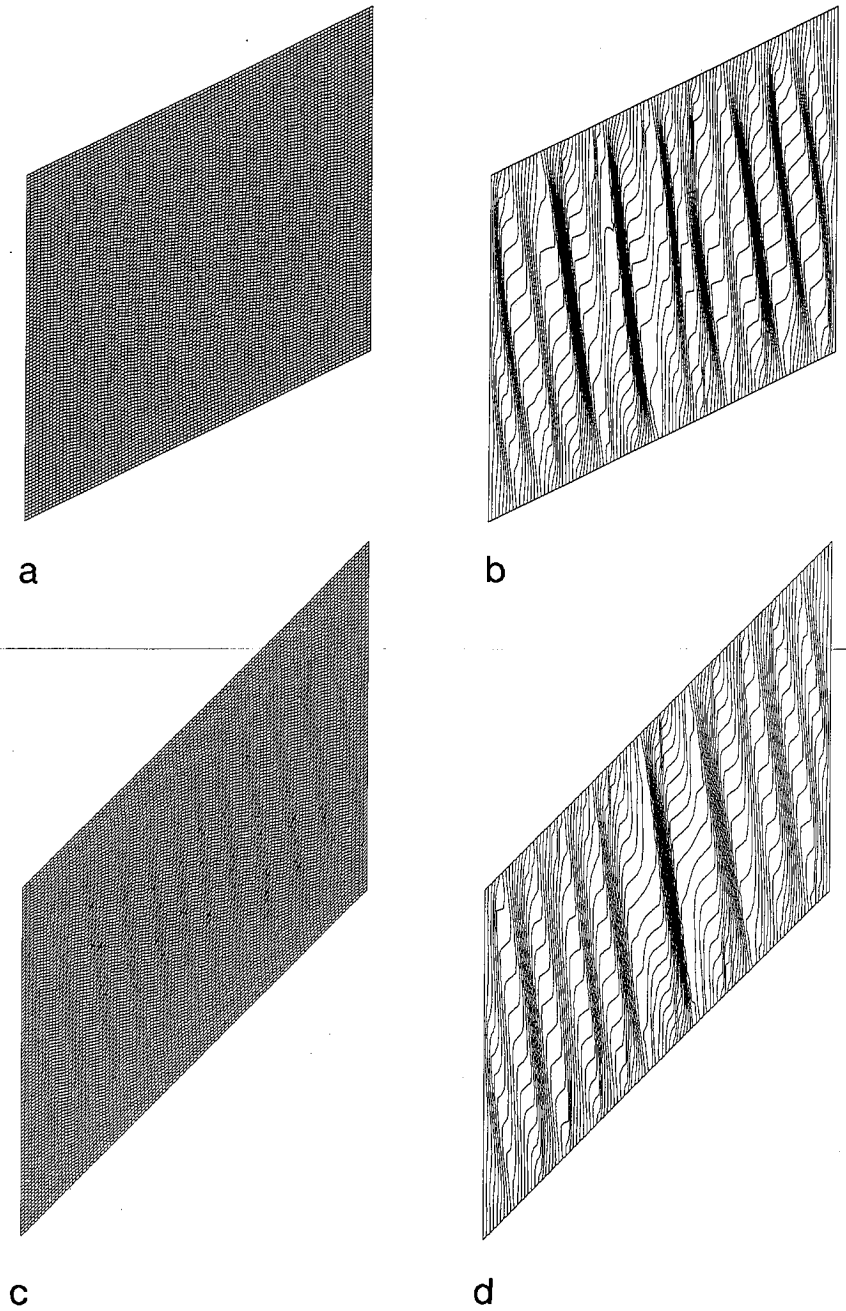

Fig. 4 a-d. 100 x 100 grid. (**a**) and (**b**) $\gamma = 0.5$. (**c**) and (**d**) $\gamma = 1.0$. (**a**) and (**c**) Sheared grids. (**b**) and (**d**) Contours of the instantaneous y-velocity. The contour interval is 5×10^{-5} units per time step in each case.

nodes were given velocities similarly, but only for the first computational step, resulting initially in an homogeneous simple shearing of the material. Thereafter, the n^2 or n x m deforming zones may dilate or contract, and undergo whatever deformation is consistent with the local kinematics and dynamics so long as the overall boundary conditions are satisfied. A total of 10 000 time steps results in a shear strain of 1.

Material Properties

The material is equivalent to that described by Hobbs & Ord (1989) in that it is isotropic and elasto-plastic with no hardening. The material follows a non-associated Coulomb constitutive law (Vermeer & de Borst 1984, Hobbs et al. 1991) as a result of the non-equality of the friction and dilation angles. The magnitudes of these angles are the same as those used in Ord (1990, 1991).

All elements have the same elastic shear modulus (1 GPa) Poisson's ratio (0.125), cohesion (10 MPa), friction angle (30°) and dilation angle (10°). One or two elements were, in some experiments, given higher elastic moduli (shear modulus of 10 GPa), but the same plastic properties. They behave as an elastically hard inclusion within a deforming mass. The shear band formation appears to be triggered by the inherent instability of the non-associated constitutive law as well as by the presence of this initial material heterogeneity, as described also by Cundall (1989, 1991). However, different positions of these elements within the grid made no difference to the stress/strain curve or to the results of the following analysis.

Results

Geometrical results only are presented. Mechanical results are described in Ord (1990), Hobbs et al. (1991) and Ord (1991).

We wish to examine the spatial distribution of one component of the system. In this instance, the component of the system is the spatial distribution of the instantaneous velocity of growth of the crenulations. The velocity of growth of the crenulations is represented by determining the velocity in the y-direction (Fig. 2), parallel to the shearing direction, for each node. The patterning of the grids, which represents a finite displacement, together with the contours of instantaneous y-velocity, are shown for shear strains of 0.5 and 1.0 in Fig.s 3 (50 x 50 grid), 4 (100 x 100 grid) and 5 (240 x 240 grid). 'Cross-sections' through these contours are shown in Fig. 6 for comparison with the results of the 10 000 x 100 grid.

The patterning appears periodic for the 50 x 50 grid, and quasi-periodic for the 100 x 100, 240 x 240 and 10 000 x 100 grids. This interpretation is confirmed by plots of both the Fourier transform and the autocorrelation of the data, as shown

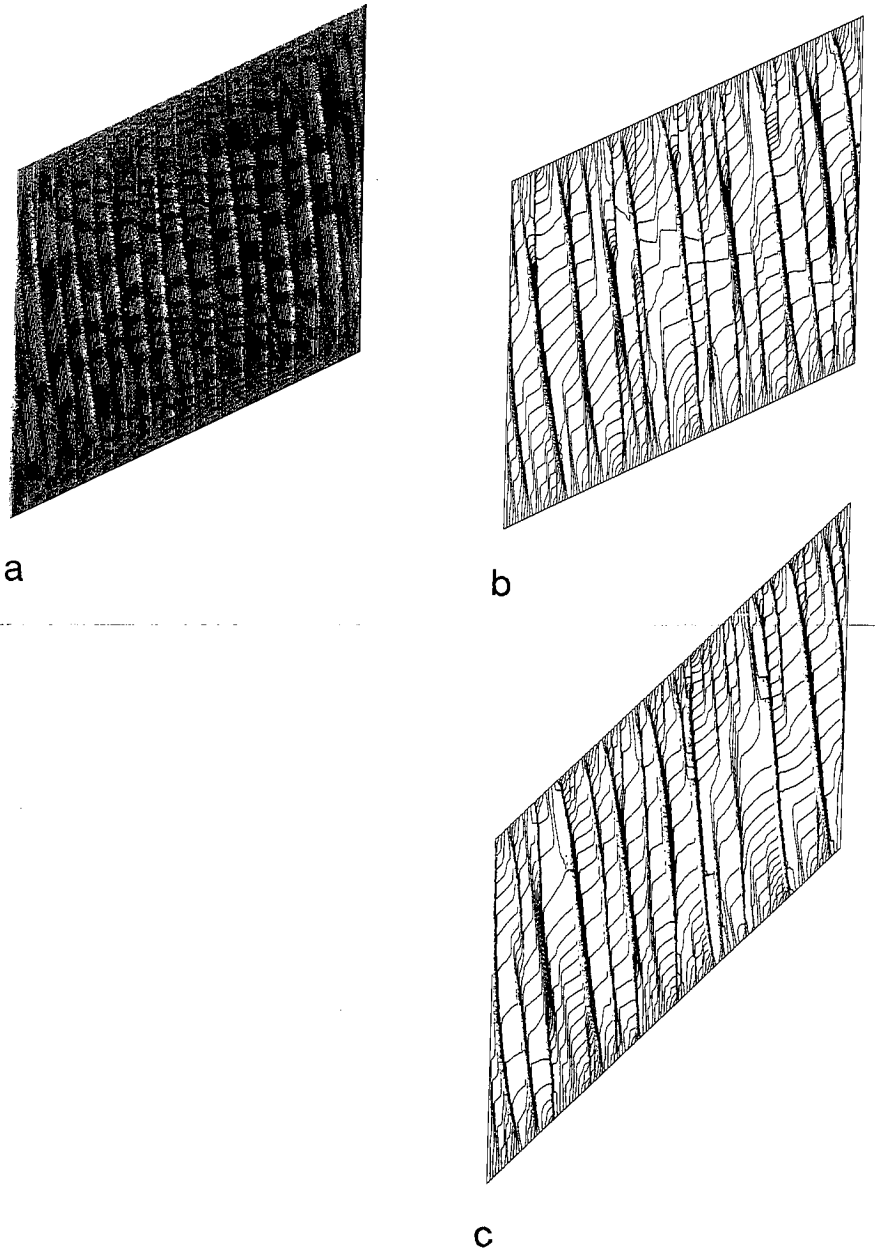

Fig. 5 a-c. 240 x 240 grid. (**a**) and (**b**) $\gamma = 0.5$. (**c**) $\gamma = 1.0$. (**a**) Sheared grid. (**b**) and (**c**) Contours of the instantaneous y-velocity. The contour interval is 1×10^{-4} units per time step in each case.

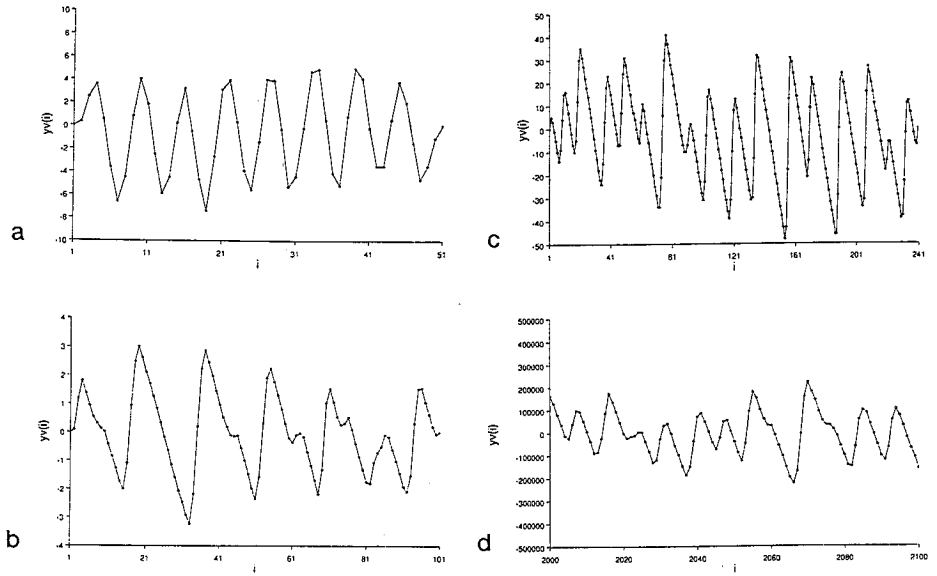

Fig. 6 a-d. Instantaneous y-velocity yv(i) versus node i for one row of each grid for a finite shear strain of 0.5. (**a**) 50 x 50 grid. row 26. (**b**) 100 x 100 grid. row 51. (**c**) 240 x 240 grid. row 121. (**d**) 10 000 x 100 grid. row 51.

in Fig. 7. Figure 8 displays variety within one row. Both the broad-banded spectrum underlying the periodic spikes of the Fourier transform and the spike at $x = 0$ of the autocorrelation increase in intensity as the grid length increases indicating an increase in wide band noise. The strong periodicity displayed in Fig. 7a-c degenerates to responses indicative of wide band noise superimposed by narrow band noise. The dominant microstructural wavelength varies from about 6 to 12 units.

Phenomena such as possible period doubling require further investigation.

We wish to determine first, if this behaviour does indeed represent the behaviour of a dynamic, self-organising system, and if it does, then how many degrees of freedom has the system?

Methodology of Dimensional Analysis

Temporally erratic behaviour has been analysed for a variety of non-linear dynamic systems; here we investigate spatially erratic behaviour. Techniques for analysis of spatiotemporal chaos have been described by, for example, Mayer-Kress & Kaneko (1989) for coupled map lattices. We construct an attractor for the spatially disposed pattern in the same way that Packard et al. (1980, see also Takens 1980, Crutchfield et al. 1986) obtained the attractor for a temporally-

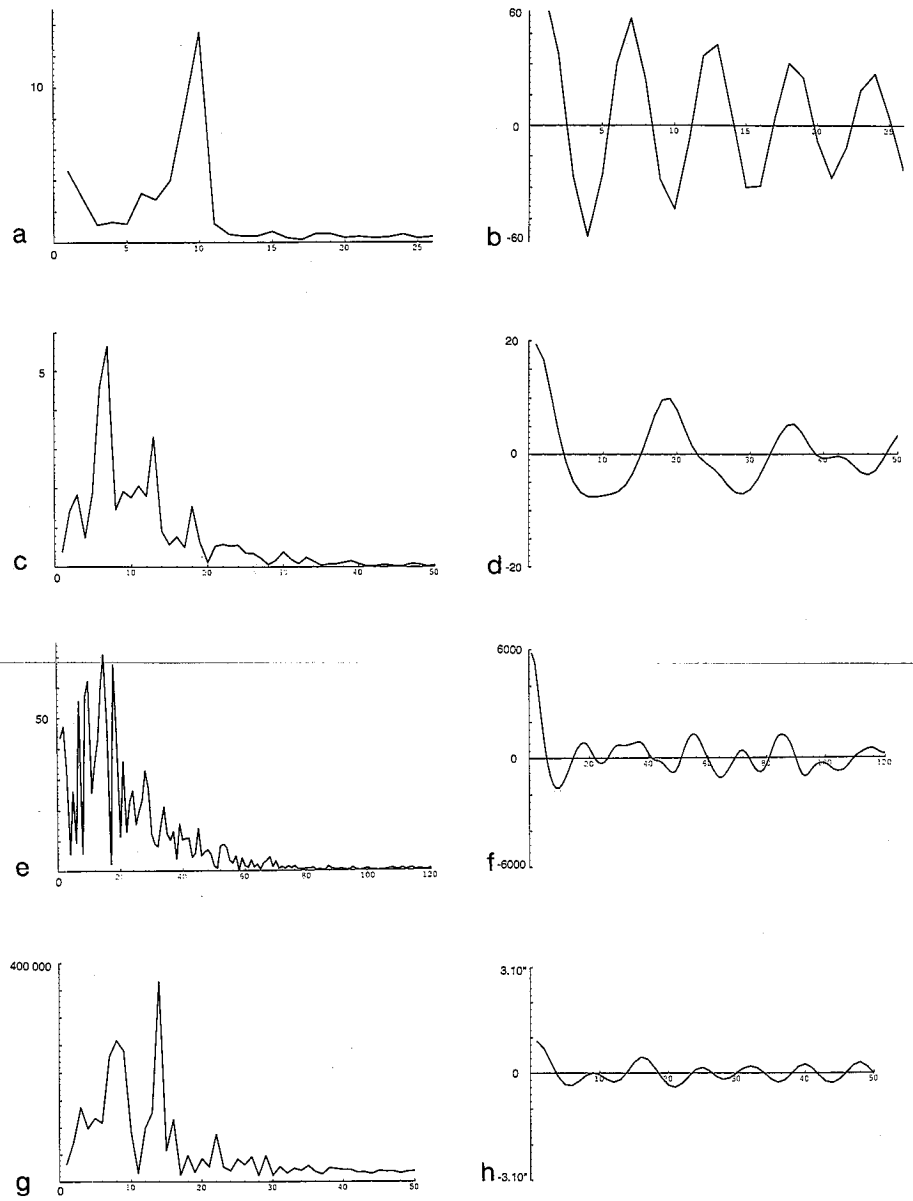

Fig. 7 a-h. Fourier transforms (**a,c,e,g**) and autocorrelations (**b,d,f,h**). (**a,b**) 50 x 50 grid. row 26. (**c,d**) 100 x 100 grid. row 51. (**e,f**) 240 x 240 grid, row 121. (**g,h**) 10 000 x 100 grid. row 51.

disposed pattern. We recognise that the evolution of one component of a system is determined by its interaction with other components, and reconstruct an

'equivalent' state space by examining the measured values at fixed space (rather than fixed time) delays with respect to a single component as though these space delays were new dimensions in this 'equivalent' state space. In this instance, the component of the system is the velocity of growth of the crenulations in the numerical modelling experiments. We are then able to examine the dimension of this spatial attractor within different embedding dimensions, and infer the dimension of the system (for a succinct review, see Ruelle 1990). The dimension of the system is representative of the number of degrees of freedom of the system, and therefore of the number of independent, non-linear differential equations required to describe the system.

This methodology is described with respect to the finite difference grid of the numerical model (Fig. 9). The magnitude of the y-velocity is provided for each grid point at each finite difference step. The identification of grid point (i, j) indices is as described in FLAC (1991, Fig. 4-3b). In this instance the space delay calculations are calculated separately for each row; that is, in terms of i, not in terms of j. However, the information obtained for all values of j is incorporated when describing the spatial phase portraits or attractors for the different embedding dimensions. The calculations may therefore be described as follows.

A single trajectory in p-dimensional 'equivalent' state space is described for i = 1, 2, ...m and j = n by constructing a space series yv(i,j), i = 1, 2, ...N; N = m - (p - 1) S by grouping p values of the space series into p-dimensional vectors

$$yv_{i,j}^{(p)} = (yv(i,j), yv(i+S,j), \ldots, yv(i+(p-1)S,j)) \qquad (1)$$

where S is the space delay, and represents an integral number of grid points, and yv(i,j) is the y component of the instantaneous growth velocity at the grid point (i,j) after subtraction of the overall homogeneous shearing. The dimension p is called the embedding dimension. The attractor for the entire model is described by allowing j to range from 1 to n.

The formation of such a spatial attractor is shown in Figure 10 for a grid size of 100 x 100 zones (101 x101 grid points). The maximum value of N is dependent on m and on p and S so that N = m - (p-1)S. Figure 10a shows the form of a single trajectory for j = 51 and S = 10, in 2 dimensions. Let the embedding dimension be 2, then N = 101-(2-1)10 = 91 so that i = 1, 91 and the axes are yv(i,51) and yv(i+10,51) or $yv_{i,51}^{(2)} = [yv(i,51), yv(i+10,51]$. The 101 trajectories for the entire grid (i=1, 91; j=1, 101) are shown in Fig. 10b. Figure 10c may be considered as a 2D section for S = 20 and p = 2, or for S = 10 and p $\geq$ 3. Similarly, Figure 10d may be considered as a 2D section for S = 30 and p = 3, or for S = 10 and p $\geq$ 4. The only difference would be in the allowed value for N. Further, Figures 10e, 10f and 11 show 3D sections, in this case unambiguously for S = 10. Again, unless N is provided, the embedding dimension can only be inferred to be at least 3 in Figure 10e and at least 4 in Figure 10f. Figure 12a shows the attractor for the 240 x 240 grid also for S = 10, and from the same viewpoint as Figure 10e.

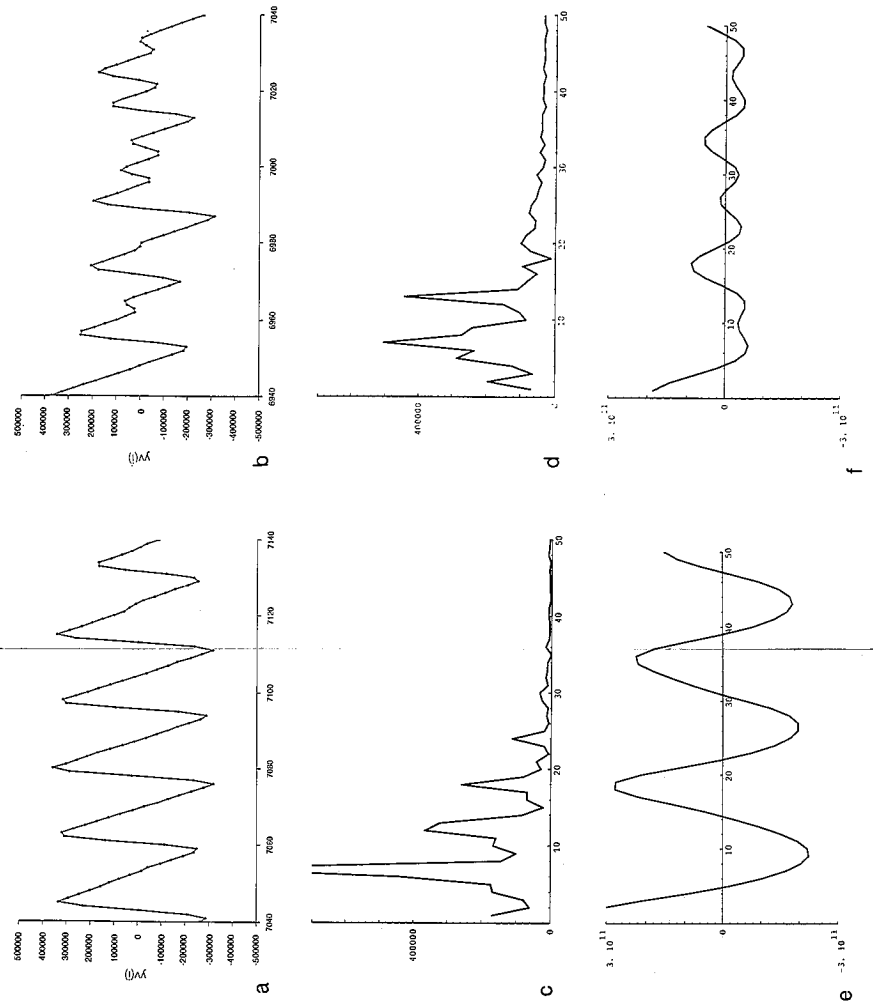

Fig. 8 e-f. 10 000 x 100 grid. Row 51 (**a,c,e**) nodes 7040 to 7140 (**b,d,f**) nodes 6940 to 7040 (**a,b**) Instantaneous y-velocity yv(i) versus node i (**c,d**) Fourier transform. (**e,f**) Autocorrelation.

A random array of 240 x 240 points is shown in Figure 12b for visual comparison of an array which fills space with one which does not fill space (Fig. 12a).

The spatial attractors for different parts of row 51 of the 10 000 x 100 grid are shown in Figure 13. There is a strong similarity between Figure 10a and Figure 13a, which should be expected from examination of Figure 10. Comparison of Figures 13a, b and c shows graphically that the attractor for a single row has

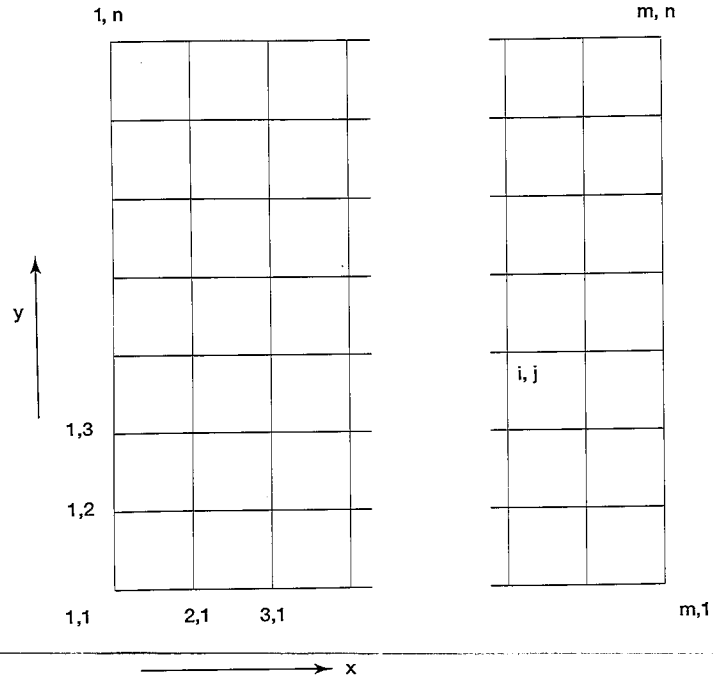

Fig. 9. Numbering system for the nodes of the finite difference grid. For the square grids m = n, and m = 50, 100 or 240. i = j = 1, m. Otherwise, m = 10 000 and n = 100. i = 1, m. j = 1, n.

structure. However, it is obviously not as well-defined as the superimposed attractors from juxtaposed rows.

These attractors are at least as aesthetically pleasing as, for example, the classic Lorenz attractor obtained from the simple equations

$$\left.\begin{aligned} \dot{x} &= \sigma(y-x), \\ \dot{y} &= \rho x - y - xz, \\ \dot{z} &= -\beta z + xy, \end{aligned}\right\} \quad \begin{aligned} &(x,y,z) \in R^3 \\ &\sigma,\rho,\beta > 0 \end{aligned}$$

These equations are used to represent fluid convection and contain three parameters, the Prandtl number, σ, the Rayleigh number, ρ, and an aspect ratio, β, as summarised by Guckenheimer & Holmes (1983). x, y and z are Cartesian coordinates and a dot denotes differentiation with respect to time. Similarities and comparisons with systems such as these provide at least some of the motivation for investigating rock deformation behaviour in terms of self-organisation and non-linear dynamics.

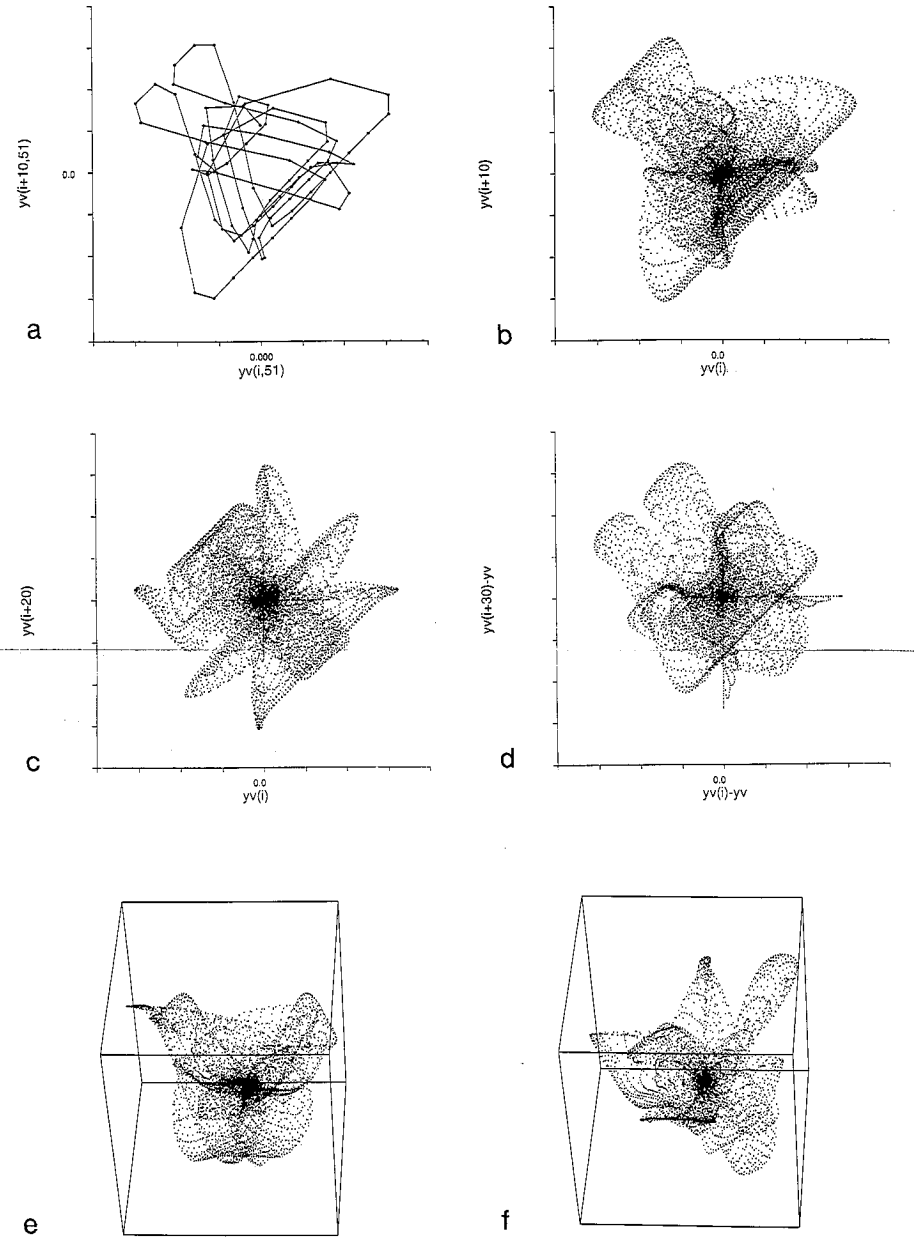

Fig. 10 a-f. 100 x 100 grid. Homogeneous shearing velocity has been subtracted so as to demonstrate only variations in y-velocity with respect to the homogeneous state. **a** single trajectory of the magnitudes of the y-velocities for j = 51 and S = 10. **b** Multiple trajectories of the magnitudes of the y-velocities for j = 1, 101 and S = 10. **c** Multiple trajectories of the magnitudes of the y-velocities for j = 1, 101 and S = 20. **d** Multiple trajectories of the magnitudes of the y-velocities for j = 1, 101 and S = 30. **e** and **f** 3D sections of multiple trajectories of the magnitudes of the y-velocities for j = 1, 101 and S = 10. Axes are yv(i), yv(i+10), and yv(i+20) for **e**, and yv(i), yv(i+10), and yv(i+30) for **f**.

The aim therefore is to use the information contained in the attractors presented here as the basis for refining our present models for the description of rock deformation behaviour.

We choose initially to determine the dimension of the spatial attractors described here by a box-counting algorithm. Different techniques (see, for example, Rasband, 1990, Chap. 4.1) may be used if the results of this initial study show that they are required.

The fractal dimension D (Mandelbrot 1977) is given by

$$D = \varepsilon \xrightarrow{\lim} 0 \ \lim \{-\ln N(\varepsilon) / \ln \varepsilon\},$$

where $N(\varepsilon)$ is the number of boxes of side ε required to cover the attractor in phase space.

This reduces to $D = -\ln N(\varepsilon) / \ln \varepsilon$, for sufficiently small ε so that the slope of a best fit straight line to ln N versus -ln ε gives D.

The numerical code follows the logic described by McGuinness (1983). The variables $yv_{i,j}^{(p)}$ are normalised so that the bounds of the attractor are 0,1 in all directions. The coordinates of the current box entered are given by dividing the $yv_{i,j}^{(p)}$ by the box side e and taking the integer part, and a "1" bit is entered when a box is entered by a trajectory on the attractor.

A CONVEX 220 with 2 processors was used for computations involving full vectorisation, and 790 Mb of real memory (Young 1991).

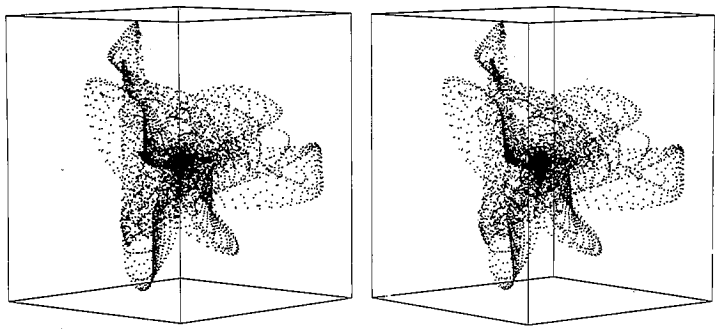

Fig. 11. Stereoscopic images of the phase portrait described in Figures 9e and 9f. Axes are yv (i), yv (i + 10), and yv (i + 20).

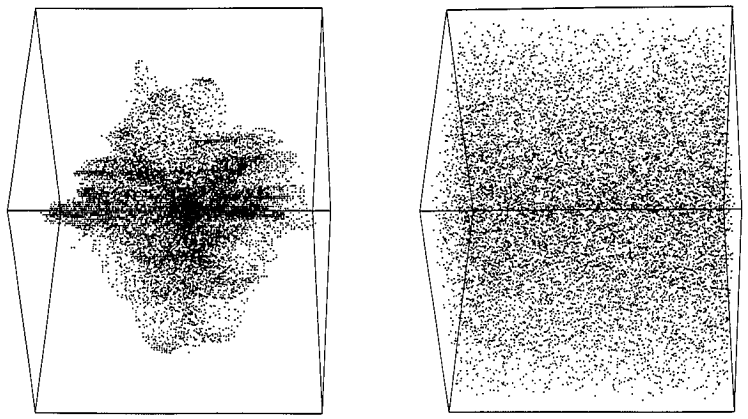

Fig. 12 a,b. a Phase portrait for the 240 x 240 grid for j = 1, 241 and S = 10. **b** Random array of 240 x 240 points. Axes are yv (i), yv (i + 10), and yv (i + 20).

For this initial investigation, the best-fit straight line to ln N versus -ln ε was chosen by eye.

The dimension of the attractor may be determined in this manner for any embedding dimension. The fractal dimension of the attractor for the entire system is the maximum limit to the dimension for the attractor as the embedding dimension is increased.

Results of Dimensional Analysis

We used the above methodology in analysis of the numerical model for different grid sizes deformed to different shear strains. The dimension of the spatial attractor for the system varies from about 2.3 to slightly less than 3.

Figure 14 demonstrates the steps involved in determination of the dimension of the system for the 100 x 100 grid. Figure 14a shows ln N versus ln ε for 10201 points of the attractor reconstructed in embedding spaces with dimensions ranging from p = 2 to p = 7 for S = 1. The magnitudes of the gradients of the best-fit straight lines sketched in Figure 14a are plotted in Figure 14b as fractal dimension D versus embedding dimension p.

Similarly, Figure 15a shows ln N versus ln ε for the 58 081 points of the 240 x 240 grid for p = 2 to p = 7 and for S = 1, and Figure 15b presents the fractal dimensions derived from the gradients of these data versus the embedding dimension.

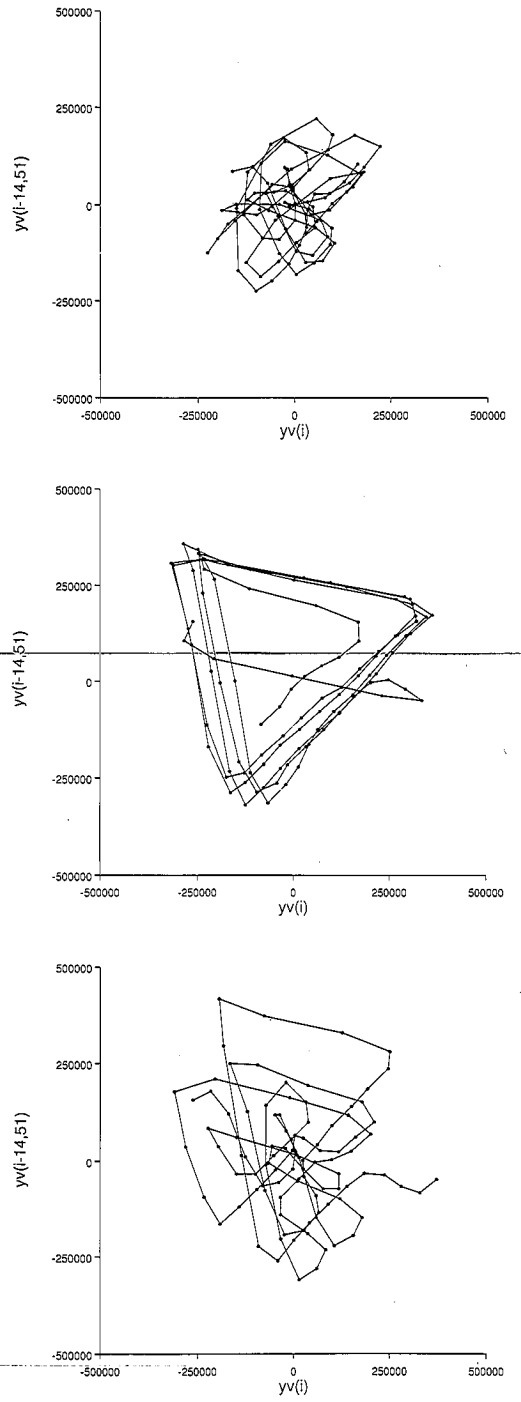

Fig. 13 a-c. Phase portraits for the 10 000 x 100 grid for j = 51. Space lag = 14.
a nodes 2000 to 2100 (Fig. 6d)
b nodes 7040 to 7140 (Fig. 8a)
c nodes 6940 to 7040 (Fig. 8b)

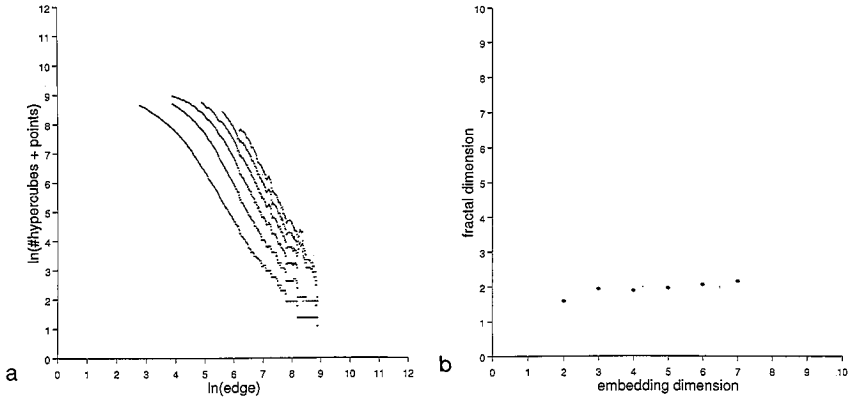

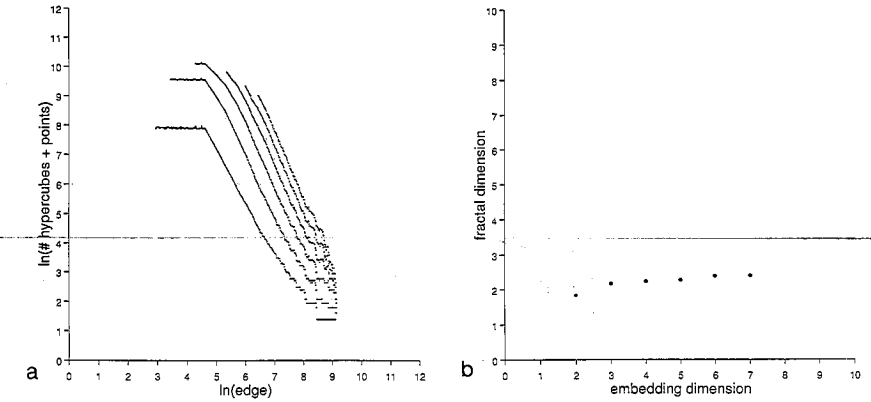

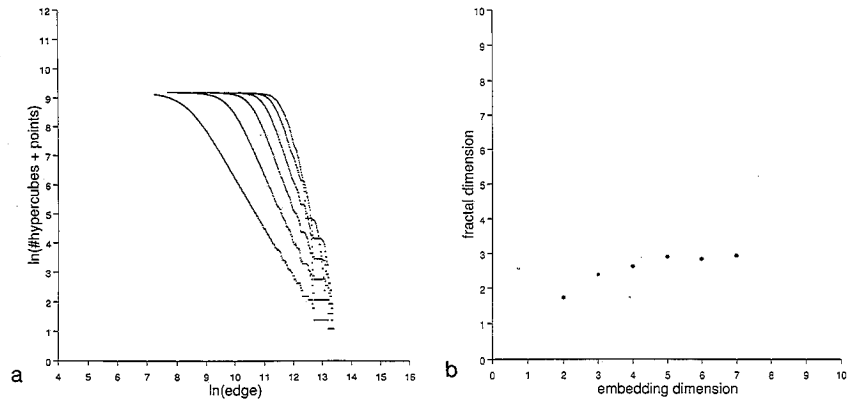

Fig. 14 a,b. (upper): 100 x 100 grid. S = 1. **a** ln N(ε) versus ln ε. **b** D versus p.
Fig. 15 a,b. (middle): 240 x 240 grid. S = 1. **a** ln N(ε) versus ln ε. **b** D versus p.
Fig. 16 a,b. (lower): 10 000 x 100 grid. row 51 S = 10. **a** ln N (ε) versus ln ε. **b** D versus p.

For comparison, Figure 16a shows ln N versus ln ε for the 10 001 points of row 51 of the 10 000 x 100 grid for p = 2 to p = 7 for S = 10, and Figure 16b presents the fractal dimensions derived from the gradients of these data versus the embedding dimension.

Figure 17 is a synoptic diagram which presents the data from Figures 14b, 15b and 16b, together with the results for S = 10 for the 100 x 100 grid and the 240 x 240 grid, and for a collection of points produced by a random process. Changing S makes no difference to the space-filling properties of the data produced by the random process. S = 10 for both the 100 x 100 and 240 x 240 grids results in D higher by at most 0.4 units than for S = 1. The grid point spacing is therefore not so close that the associated instantaneous y-velocities represent the same information. S = 10 was chosen as approximating the wavelength of the crenulations (as determined from Figs. 6 and 7) and maximising the information on the attractor. Also, there are not enough points to investigate the system for values of S greater than 10. D is also slightly higher for the 240 x 240 grid than for the 100 x 100 grid. This appears to be a result of the larger number of points and the more clearly defined region of constant slope.

The following points arise from this analysis:

a) For large values of ε the slope of ln N versus ln ε tends to 0 since when ε is larger than the size of the attractor, all the points of the attractor are contained in the target hypercube.

b) As ε approaches zero, the attractor progressively loses resolution as ε approaches the numerical precision with which the position of individual points is known.

c) The fractal dimension of the attractor in any embedding dimension must be determined over some intermediate range of ln ε that shows a stable constant slope (the scaling region), preferably over 2 or 3 orders of magnitude. Ruelle (1990) notes that gradients for a slope determined over less than a decade seem unreasonable. Figure 14b is then a plot of the slope of ln N versus ln ε over the range of ln N between roughly 3 and 8.

d) As described above, the fractal dimension of the system is represented by the constant value to which the dimension of the attractor converges as the embedding dimension is increased. This value varies from about 2.3 almost to 3 as shown in Figure 17. This satisfies the requirement described by Takens (1981) that the fractal dimension F of a system must be obtained by investigation into an embedding space of at least 2F+1, i.e. $p \geq 2F+1$. For F = 3.0, $p \geq 7.0$, and we have investigated p up to a value of 7.

e) Number of samples needed to define the attractor adequately. As the number of points is decreased, the population of points at small scales becomes increasingly diffuse, resulting in large fluctuations of ln N which can completely mask the scaling region. In analysis of the reliability of results for the Grassberger-Procaccia algorithm, Ruelle (1990) infers that the total number of points examined, N, should be greater than D according to $2\log_{10}N \geq D$. Applying this to our results, our maximum D is 3.0. For N only

5000, $2\log_{10}N = 7.4$. So the results from row 51 (10001 points) of the 10000 x 100 grid and from the 100 x 100 (10261 points) and 240 x 240 (58081 points) grids may be worth considering.
Further, as the calculation of N shows, embedding a fixed number of points into higher and higher dimensions effectively reduces the number of points for which the fractal dimension of each embedding space is calculated. This also results in a poorly defined scaling region.

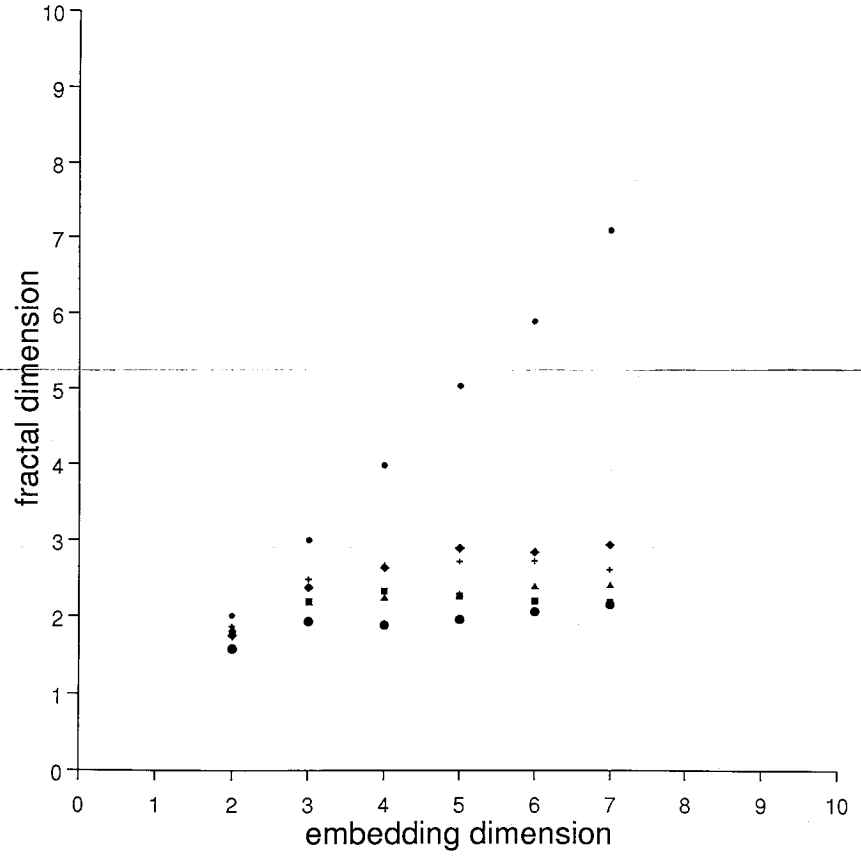

Fig. 17. Synoptic diagram Random points. Small circles. S = 1 and S = 10. 100 x 100 grid. Filled circles S = 1. Filled squares S = 10. 240 x 240 grid. Filled triangles S = 1. Crosses S = 10. 10000 x 100 grid. row 51. Filled diamonds S = 10.

Conclusions

i) A clearly-defined attractor has been described for the first time for a natural system with spatially quasi-periodic behaviour.
ii) A fractal dimension may be derived for this attractor using a box-counting algorithm.
iii) This fractal dimension varies from about 2.3 up to 3, determined for a maximum embedding dimension of 7, and for data sets of 10201 and 58081 points.
iv) It is inferred from this analysis that three first order, non-linear, independent, ordinary differential equations are required to describe this system.
v) We infer, to be consistent with the numerical model, that these are the stress equations of motion, the yield criterion and the flow rule. Although the analysis of the full non-linear problem for folding has not yet been carried out, we infer that it is the feedback relations between these three non-linear equations that leads to the observed quasi-periodicity in the velocity of growth of the crenulations described here and to the resultant quasi-periodicity in the resulting geometries. We conclude that geological systems may be analysed using the concepts of fractal geometry thus providing the basis for inferences as to the number of ordinary differential equations involved in the development of the system The treatment presented here forms the basis for a new way of viewing the irregularity inherent in geological structures and relating this irregularity to the kinematics and dynamics involved in the development of those structures.

Acknowledgements. I thank Bruce Hobbs for his continuing support of this work, ITASCA Consulting Group for continuing access to FLAC, and Bruce Hobbs, Hans Mülhaus and Frank Horowitz for their critical and positive comments on this manuscript.

References

Albano AM, Abraham NB, Guzman GC de, Tarroja MFH, Bandy DK, Gioggia RS, Rapp PE, Zimmerman ID, Greenbam NN, Bashore TR (1986). Lasers and brains: complex systems with low-dimensional attractors. In: Mayer-Kress G (ed) Dimensions and Entropies in Chaotic Systems . Springer, Berlin Heidelberg New York, pp. 231-240.

Biot MA (1961). Theory of folding of stratified viscoelastic media and its implication in tectonics and orogenesis. Geol Soc Am Bull 72: 1595-1620.

Board M (1989). FLAC (Fast Lagrangian Analysis of Continua) Version 2.20. Vol.1, Software Summary. Prepared for Division of High-Level Waste Management, Office of Nuclear Material Safety and Safeguards, NUREG/CR-5430. Washington, D.C., USA.

Chouet B, Shaw HR (1991). Fractal properties of tremor and gas piston events observed at Kilauea Volcano, Hawaii. J Geophys Res 96: 10177-10 189.

Crutchfield JP, Farmer JD, Packard NH, Shaw RS (1986). Chaos. Scientific American, 255 (6): 38-49.

Cundall PA (1989). Numerical experiments on localization in frictional material. Ingenieur-Archiv 59: 148-159.

Cundall PA (1991). Shear band initiation and evolution in frictional materials. In: Mechanics Computing in 1990's and Beyond (Proceedings of the Conference, Columbus, Ohio, May 1991), Vol. 2: Structural and Material Mechanics, pp. 1279-1289, ASME New York.

Cundall PA, Board M (1988). A microcomputer program for modelling large-strain plasticity problems. In: Numerical Methods in Geomechanics (Innsbruck, 1988), Vol 3, Balkema, Rotterdam, pp. 2101-2108.

FLAC (1991). Fast Lagrangian Analysis of Continua. Version 3.0. Volume I : User's Manual. Volume II : Verification Problems and Example Applications. ITASCA Consulting Group, Inc. Minnesota, USA.

Gollub JP, Swinney HL (1975). Onset of turbulence in a rotating fluid. Phys Rev Lett 35: 927-930.

Guckenheimer J, Holmes P (1983). Nonlinear oscillations, dynamical systems and bifurcations of vector fields. Springer, New York Berlin Heidelberg.

Hobbs BE (1990). Chaotic behaviour of frictional shear instabilities. Proc. 2nd Int. Symp. on Rockbursts and Seismicity in Mines. Minneapolis, 8-10 June 1988. Ed. C. Fairhurst, Balkema, Rotterdam.

Hobbs BE, Ord A (1989). Numerical simulation of shear band formation in a frictional-dilational material. Ingenieur-Archiv 59: 209-220.

Hobbs BE, Mühlhaus H-B, Ord A (1991). Instability, softening and localization of deformation. In: Knipe RJ & Rutter EH (eds) Deformation Mechanisms, Rheology and Tectonics. Geol Soc Spec Pub 54, The Geological Society, London, pp. 143-165.

Holmes P (1990). Nonlinear dynamics, chaos, and mechanics. Appl Mech Rev 43: S23-S39.

Lorenz EN (1963). Deterministic non-periodic flow. J Atmos Sciences 20: 130-141.

Lorenz EN (1979). On the prevalence of aperiodicity in simple systems. In: Global Analysis (Eds. M. Grmela and J.E. Marsden). Lect Notes Math **755**, Springer, New York, pp. 53-75.

Mandelbrot BB (1977). Fractals: form, chance, and dimension. Freeman, San Francisco.

Mayer-Kress G, Kaneko K (1989). Spatiotemporal chaos and noise. J Stat Phys 54: 1489-1508.

McGuinness MJ (1983). The fractal dimension of the Lorenz attractor. Phys Lett 99A: 5-9.

Ord A (1990). Mechanical controls on dilatant shear zones. In: Knipe RJ & Rutter EH (eds) Deformation Mechanisms, Rheology and Tectonics. Geol Soc Spec Pub 54, The Geological Society, London, pp. 183-192.

Ord A (1991). Fluid flow through patterned shear zones. In: Beer G Booker JR & CarterJP (eds) Computer Methods and Advances in Geomechanics Proc. 7th Intl Conf on Computer Methods and Advances in Geomechanics, Balkema, Rotterdam, pp. 393-398.

Packard NH, Crutchfield JP, Farmer JD, Shaw RS (1980). Geometry from a time series. Phys Rev Lett 45: 712-716.

Ramberg H (1964). Selective buckling of composite layers with contrasted rheological properties; a theory for simultaneous formation of several orders of folds. Tectonophysics 1: 307-341.

Rasband SN (1990). Chaotic Dynamics of Nonlinear Systems. John Wiley and Sons, New York.

Ruelle D (1990). Deterministic chaos: the science and the fiction. The Claude Bernard Lecture, 1989. Proc R Soc Lond A427: 241-248.

Sornette A, Dubois J, Cheminee JL, Sornette D (1991). Are sequences of volcanic eruptions deterministically chaotic? J Geophys Res 96: 11931-11945.

Takens F (1981). Detecting strange attractors in turbulence. In: Rand DA & Young L-S (eds). Dynamical Systems and Turbulence. Lecture Notes in Mathematics 898, Springer, New York, pp. 366-381.

Van der Pol B (1927). Forced oscillations in a circuit with nonlinear resistance (receptance with reactive triode). London, Edinburgh, and Dublin, Phil Mag 3: 65-80.

Vermeer PA, de Borst R (1984). Non-associated plasticity for soils, concrete and rock. Heron, 29(3): 1-64.

Young P (1991). Convex 200 humbled by CSIRO program. Computerworld Australia 14: No.23, 1, 6.